Chapter 18

Fluorite Crystals with Color Centers: A Medium for Recording Extremely Stable but Broadly Transformable Holograms

Aleksandr I. Ryskin, Aleksandr E. Angervaks and
Andrei V. Veniaminov

Additional information is available at the end of the chapter

http://dx.doi.org/10.5772/66114

Abstract

The mechanisms of (i) forming the photochromic color centers in fluorite crystals ("additive coloring") and (ii) recording and transforming holograms through the use of their photochromism are described here. The diffusion-drift mechanism of hologram recording in additively colored fluorite crystals determines the recording kinetics and properties of holograms. An important feature of holograms recorded in additively colored fluorite is an opportunity to perform the photothermal transformation of color centers under the incoherent optical radiation that results in nondestructive switching of the hologram between the amplitude, amplitude-phase (in-phase or counter-phase), and phase types at a given readout wavelength. Possible applications of holographic elements based on the additively colored fluorite crystals are discussed.

Keywords: fluorite crystal, additive coloring, color center, colloids, transformation, holography, diffraction efficiency, kinetics, profile

1. Introduction

Holographic elements are broadly used in the laser technique for spectral narrowing, stabilizing, and tuning the laser emission, phase locking in resonators, angular narrowing and steering the laser beams, stretching, compressing, and shaping the laser pulses, and also in combining laser beams. These applications impose specific requirements in holographic media. One of important requirements is their stability to the effects of optical radiation and temperature. Another useful feature is the transparency in the infrared because IR lasers are

widely used in the modern techniques. In this paper, a holographic medium is described that satisfies both these requirements: it is extremely stable and allows for reading out holograms in the IR up to ~10 μm. This medium is calcium fluoride crystals (CaF_2, fluorite) with color centers. Color centers in fluorite are the combination of anion vacancies and electrons trapped by the latter; the centers exhibit the absorption bands in the visible region and, thus, color the crystal. To form the centers in the crystal bulk, heating the crystal in the reducing atmosphere of calcium vapor is used (so-called "additive coloring" of the crystal). Color centers can also be created in the crystal volume under the impact of γ-radiation or high-energy electron beams; however, such coloration is less stable.

The photochromism of colored crystals that allows for their use as a holographic medium is due to the transformation of color centers under the illumination of the crystal in the absorption band of specific center at an elevated temperature.

In this paper, the technique of additive coloring of fluorite crystals is described. The types of color centers are discussed as well as their photochromic transformations. Special attention is paid to the mechanism of hologram recording because it is this mechanism that determines the most important features of holograms recorded in this medium. The phenomenon of self-organization of color centers under hologram recording is considered. In conclusion, possible applications of the medium are discussed.

2. Additive coloring of fluorite crystals

As mentioned above, the color centers in fluorite crystals are anion vacancies that capture electrons. The additive coloring procedure is executed in gas-controlled heat pipe [1, 2]. The essence of heat-pipe method that implies the use of furnace and water-cooled refrigerator (**Figure 1**) is in the spatial separation of a buffer inert gas (He) and metal vapor due to vertically directed metal diffusion at the temperature gradient formed by the furnace and the refrigerator. The metal vapor is condensed on the manipulator rod at a dew point temperature in a zone above the container with the crystal, drains to the hot zone and evaporates in it. As a result, the vapor-gas mixture pressure is determined by the pressure of He that is in equilibrium with the metal vapor, thus being almost independent of the temperature of a sample under coloration.

The dynamic mode of the heat pipe—continuous circulation of metal vapor within it—is implemented at a fairly low pressure of saturating metal vapor at its freezing temperature. This condition is not satisfied for calcium, but is fulfilled for alkali metals. Therefore, a calcium-lithium mixture (*10*) is used to implement the aforementioned mode. In this case, the dew point is determined by lithium that dominates in the mixture composition (~99%), and the coloring agent is calcium vapor.

Thus, the heat-pipe method allows one to control the calcium vapor pressure, p, and temperature, T, of the colored crystal almost independently. The ranges of the parameter magnitudes are as follows: $p = 10^{-4}$–1 Torr, $T = 730$–870°C.

http://dx.doi.org/10.5772/66114

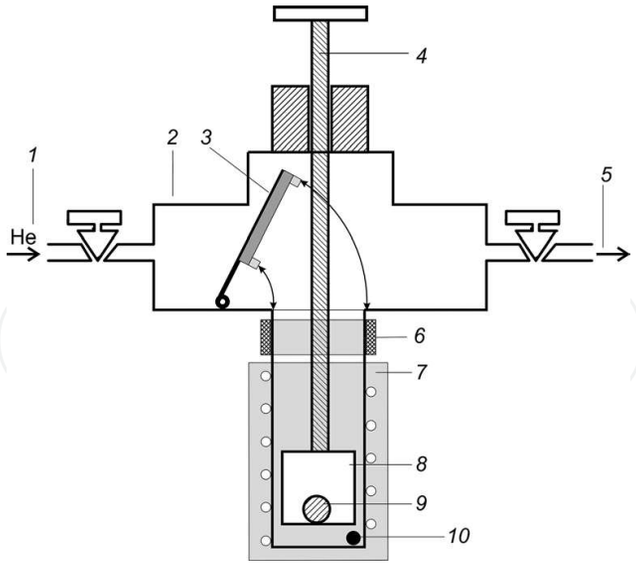

Figure 1. Schematic representation of the heat-pipe system: (*1*) helium supply, (*2*) stainless steel vacuum chamber, (*3*) vacuum valve, (*4*) manipulator for displacing the container with a sample, (*5*) line to the vacuum pump, (*6*) water-cooled refrigerator, (*7*) furnace, (*8*) container, (*9*) sample, and (*10*) metal weight.

About several tens of coloring procedures can be implemented, with reproducible results, using the same lithium-calcium weight.

The formation of color centers under the additive coloring is related to the deviation of the crystal from stoichiometry. The crystal surface builds up when interacting with metal vapor and using anions borrowed from the crystal bulk. In other words, the anion vacancies diffuse into the crystal simultaneously with electrons supplied by calcium to support the charge neutrality of the colored sample. One should note that, at sufficiently high coloring temperature, the surface undergoes decomposition (erosion). During this process, the metal cations pass to the gas phase at a low vapor pressure and remain on the crystal surface at pressures close to the saturation vapor pressure. Fluorine that evolved during the surface layer decomposition recombines with anion vacancies formed as a result of the interaction with the metal film on the surface. Thus, from the viewpoint of crystal stoichiometry violation, these two reactions, namely, the surface building up and decomposition, are oppositely directed. One should note that, for CaF_2 crystal, the process of building-up the surface prevails over its decomposition.[1]

The recombination of anion vacancies and electrons diffusing into the crystal bulk produces a variety of color centers. The method used allows for the uniform coloring of CaF_2 crystals of a large size (**Figure 2**).

After the furnace is switched off in the end of the coloring procedure, the crystal cools down to the room temperature; a minute quantity of oxygen present in helium penetrates, because

[1]This is not the general case; for example, in CdF_2 crystal that has the fluorite structure, the rates of both processes are comparable and the surface of additively colored crystals turns out to be greatly eroded.

of absence of Ca vapor, into the surface layers of colored crystal and substitutes fluorine ions for the O_2^- ions with electrons borrowed from the color centers. So, the surface layers of the crystal become partially discolored. For hologram recording, plates of uniformly colored inner part should be cut out and polished.

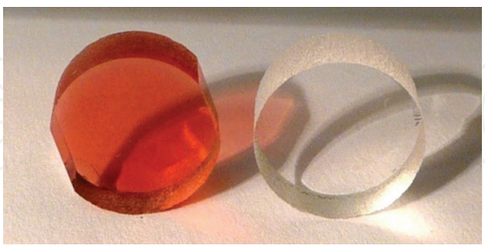

Figure 2. Samples of fluorite crystals 12 mm in diameter and 6 mm thick: initial (right) and additively colored (left).

To form color centers that consist of anion vacancies and electrons, it is necessary to use high-purity and high-quality fluorite crystals. Luckily, fluorite is an important material of photolithography optics used together with excimer lasers for semiconductor chip production, which is why the technology of growing such crystals is well elaborated. So, such crystals are available and not expensive.

3. Color centers and their photothermal transformation

Color centers in fluorite crystals may be separated into three groups. "Simple" centers are those comprising 1–4 anion vacancies and equal number of trapped electrons (*F*-, *M*-, *R*-, and *N*-centers, respectively); the structure and energy levels of simple centers in fluorite crystals are well studied [3]. "Colloidal" centers (colloids) are the giant agglomerates of vacancies and electrons converted, at the coloring temperature, into the metal calcium drops less than ~50 nm in diameter (its value depends on the coloring mode). "Quasi-colloidal" centers occupy, by the number of vacancies/electrons, an intermediate position between simple and colloidal centers; probably, they are more or less large agglomerates of simple centers.

All centers are characterized by the specific absorption bands. The bands of simple centers are located in the $\lambda < 550$ nm wavelength range. The extinction of colloidal centers is well described by Mie theory [4–6]; the visible band of these centers is located in the 500 nm $< \lambda <$ 600 nm range depending on the coloring mode (the second band of colloidal centers is located at ~200 nm). There is a lot of quasi-colloidal centers, their bands covering a wide spectral range, 550 nm $< \lambda <$ 10 μm. The bigger the quasi-colloidal center, the closer its absorption band to the band of colloids [7].

The modification of coloring conditions (calcium-vapor pressure and temperature) determines the composition of color centers in the colored crystal. The higher the calcium pressure the larger the amount of colloidal particles formed (**Figure 3**); their size increases with an increase

http://dx.doi.org/10.5772/66114

in their concentration in the colored crystal. Only a minute quantity of quasi-colloidal centers arises during the coloring process because they are less stable compared to the simple and colloidal centers and cannot exist at the coloring temperature.

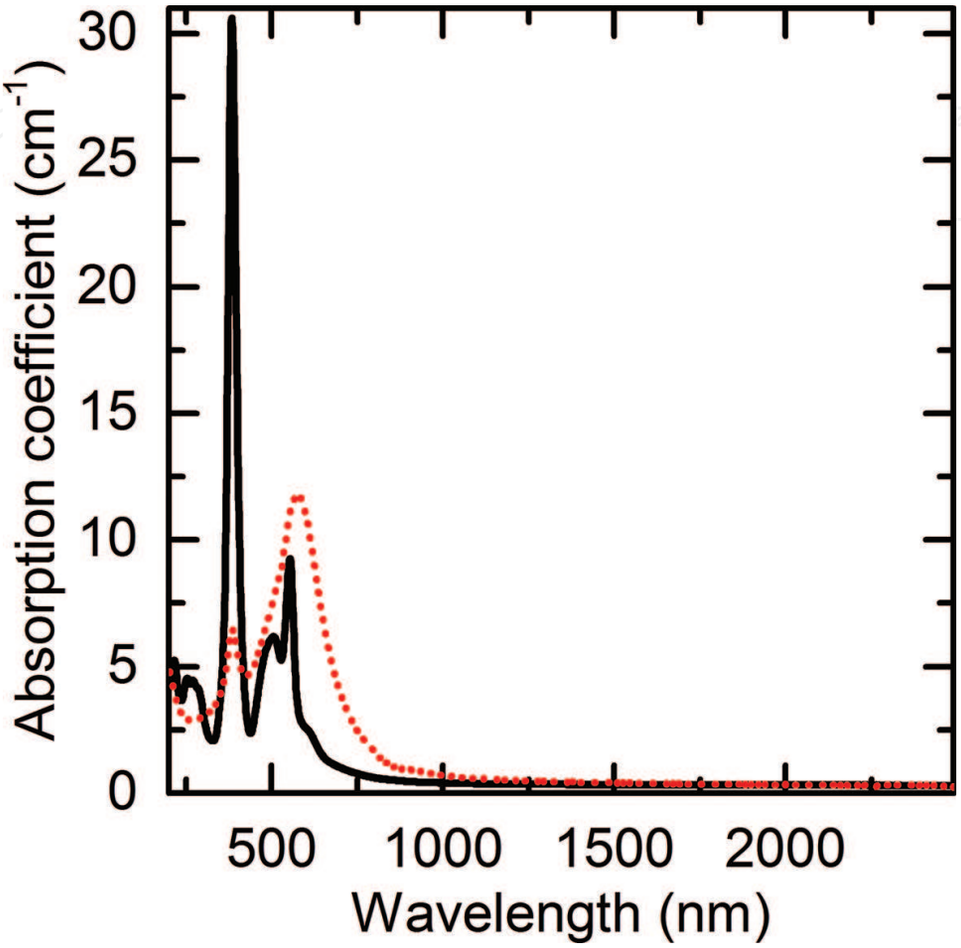

Figure 3. Absorption spectra of 2.4 mm-thick CaF_2 crystals colored at temperature T = 830°C and pressure p equal to (i) 3×10^{-4} Torr ("weakly colored," solid line) and (ii) 8×10^{-3} Torr ("strongly colored," dotted line).

Temperature determines the coloring time, but it also plays an important role in determining the composition of color centers present in the crystal in another aspect. The illumination of crystal by radiation resonant to the absorption band of a specific center at elevated temperature results in the destruction of this center and formation of another type of centers. This type crucially depends on temperature. $T > 300$°C is favorable for the simple center formation because of high entropy of these centers. At T = 150–200°C, the colloidal centers arise. The 70–150°C temperature range is favorable for the quasi-colloidal center formation. The lower temperatures of this range correspond to the formation of long-wavelength quasi-colloids; at higher temperatures, the short-wavelength quasi-colloids arise (**Figure 4**).

Photochromism of color centers in additively colored CaF_2 crystals allows for hologram recording on the crystals.

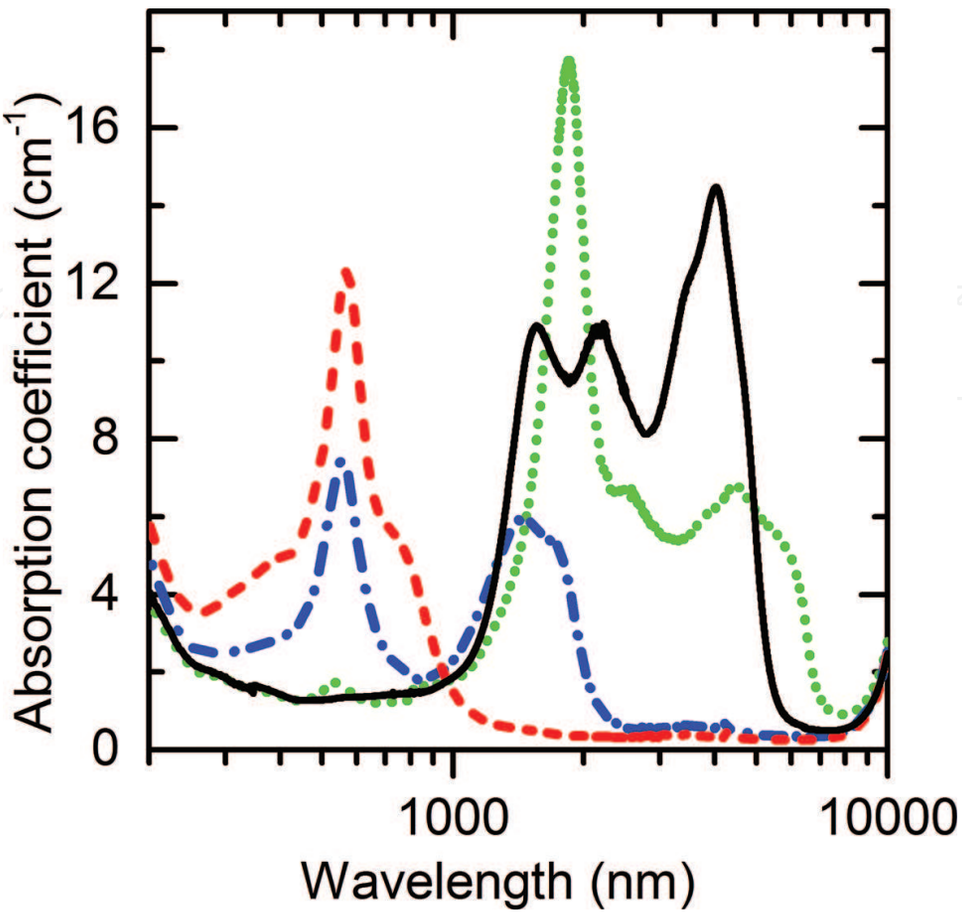

Figure 4. Absorption spectra of samples additively colored ($p = 3 \times 10^{-4}$ Torr and $T = 830$°C) and irradiated for 30 hours with the high-pressure mercury lamp ($\lambda = 365$ nm) at $T = 70$, 85, 125, and 160°C (solid, dotted, dashed-dotted, and dashed lines, respectively).

4. Mechanism and kinetics of hologram recording

When recording a hologram, the crystal and optical scheme of interferometer beginning with the beam splitter are placed into the temperature-controlled windowed housing equipped with a heater and a thermocouple. The feedback circuit of the heater power supply maintains a temperature in the housing of 150–200°C with an error of 0.1°C.

The specific diffusion-drift mechanism of hologram recording in ionic crystals with color centers [8–10] results not only in the transformation of the types of centers but also in their spatial redistribution over the crystal bulk. This mechanism is similar to Dember effect in semiconductors. If there are two carrier types with different mobilities in a semiconductor, its illumination with inhomogeneous light field results in the concentration gradient of more mobile carriers. The perturbation in local neutrality of the crystal forms local electric fields. Dember effect is responsible for the appearance of bulk charge when the mobilities of electrons and holes differ from one another.

A similar phenomenon occurs in ionic crystals with color centers. Two components that arise under the impact of light field in a crystal with color centers at elevated temperatures, i.e.,

electrons and anion vacancies, differ greatly in mobilities. Photoionization of the centers in the maxima of the fringe pattern gives birth to the free electrons that diffuse towards the minima, where they are captured by traps (the same color centers). This process creates electric fields between the minima and maxima. Under the impact of these fields, vacancies that are split off the photoionized centers at the recording temperature, drift towards minima and recombine with electrons released from traps with the formation of new color centers. Thus, the holographic planes coincide with the minima of the fringe pattern. A resultant increase in the vacancy and electron concentrations in minima compared to their mean concentrations in the sample favors the formation of colloidal centers.

Generally, the hologram recording process is linked to the simple → colloidal center conversion. This conversion in the holographic planes and the depletion of centers between them create the modulation of optical constants of the crystal, i.e., forms the holographic grating. One should note that, actually, the conversion process passes through several stages in accord with an increase in the number of center components: simple centers → long-wavelength quasi-colloids → short-wavelength quasi-colloids → colloids; of course, this scheme is simplified with allowance for the occurrence of several kinds of simple centers and a lot of kinds of quasi-colloidal centers.

According to the preceding section, the use of reverse colloidal → simple center process for hologram recording requires substantially high temperature of the crystal.

The most suitable laser wavelength for hologram recording is less than 500 nm; however, the radiation with λ = 532 nm is also effective though it is absorbed by both simple and colloidal centers (as mentioned above, the temperature range of 150–200°C is favorable for colloidal center formation).

One should note that the hologram recording in CaF_2 crystals with color centers is a dynamic process. At the recording temperature, the thermal dissociation of color centers in the minima of fringe pattern occurs, thus resulting in the formation of the "counter-flows" of electrons and vacancies towards the maxima of the fringe pattern. The study of ESR and dielectric constants of CaF_2 crystals irradiated with electrons shows that the most stable colloidal color centers break up and form at temperature above 150°C [11].

Thus, the hologram decay occurs simultaneously with its recording. With a decrease and increase in the center concentration in the interference field maxima and minima, respectively, the rates of recording and decay processes equalize, so that the diffraction efficiency of recorded hologram, DE, reaches saturation. As seen, such situation differs from that for media in which the laser radiation produces the irreversible modification (modulation) of the optical constants. This results in a decrease in DE, after passing a maximum, with an increase in exposure because of occurrence of the scattered radiation.

In **Figure 5**, the recording kinetics for the first diffraction order of the hologram read out at 980 nm is presented. The readout beam was switched on, each 10 s, for 0.1 s. The absorption spectra of the crystal registered before and after hologram recording are shown in **Figure 6**.

The hologram may be considered as the phase one with only minor amplitude contribution. However, this is the case only at the initial stage of the formation of the holographic planes. Let us consider this stage in more detail.

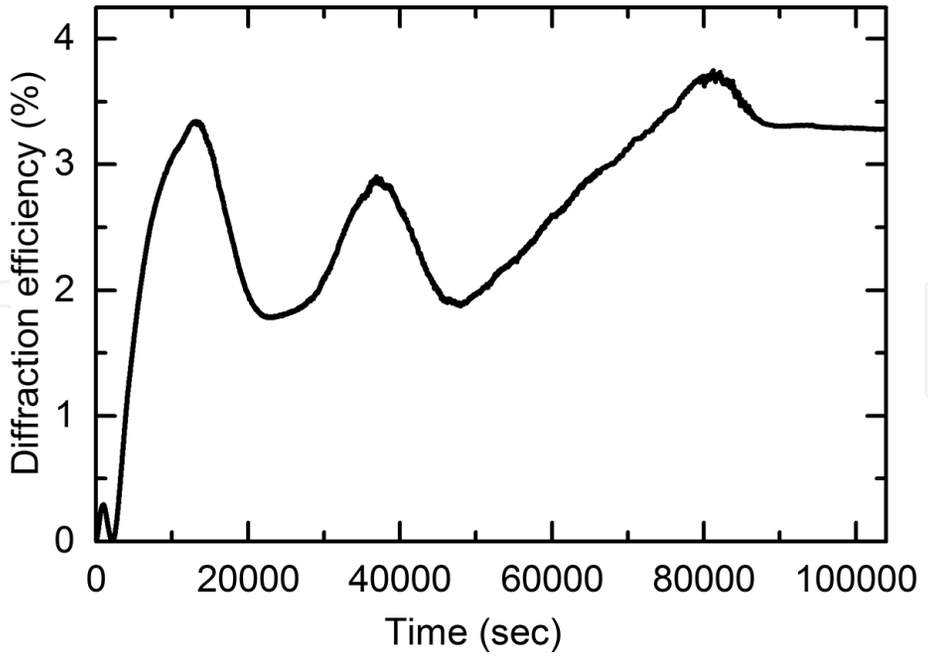

Figure 5. Diffraction efficiency measured at 980 nm vs. exposure time in the course of hologram recording with 532 nm laser emission.

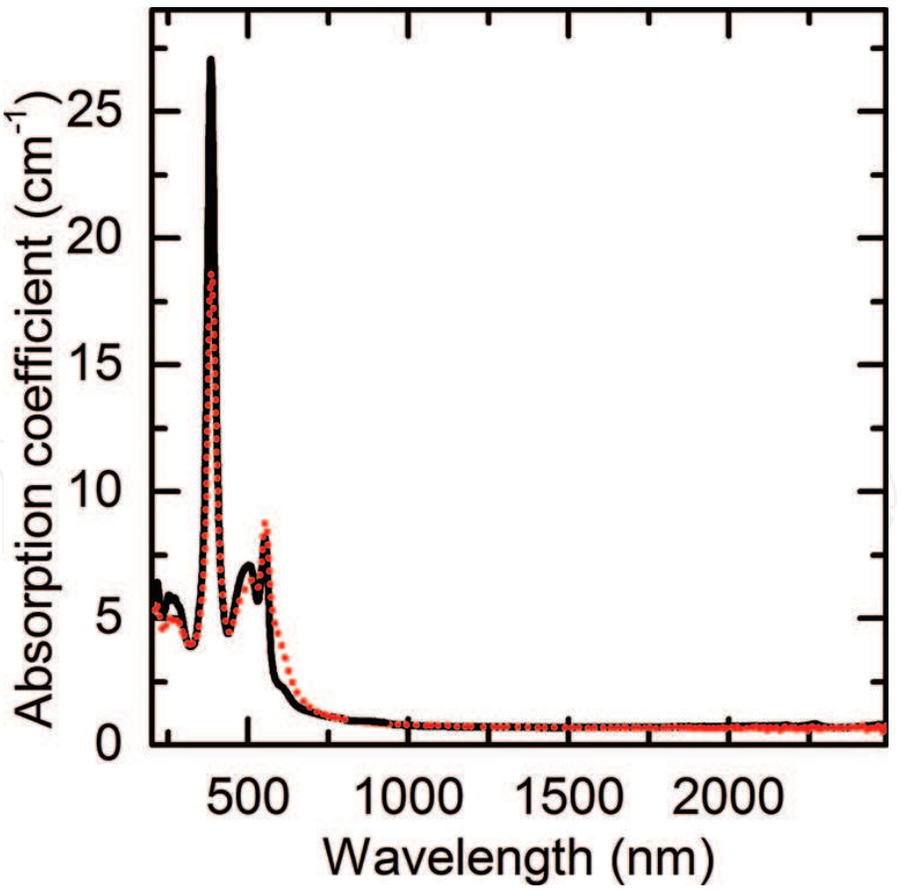

Figure 6. Absorption spectra of additively colored sample of CaF_2 crystal before (solid line) and after (dotted line) recording the "saturated" hologram.

http://dx.doi.org/10.5772/66114

The first (small) maximum of kinetic curve is related to the local center transformation in the maxima of the fringe pattern. The simultaneously occurring process of center drift from the maxima to the minima restricts an increase in DE due to the local transformation and is the reason for the appearance of the first minimum (an analogous local maximum was observed under hologram recording in KCl crystals with color centers [12]). At this point, the amount of anion vacancies/electrons is a bit larger in the minima of the fringe pattern; however, this increase is compensated by center transformation in the maxima.

A subsequent increase in the center concentration in the minima implies DE to increase up to the second maximum. The time (exposure) at which this maximum is reached corresponds to the completion of holographic plane formation.

To explain the existence of two very pronounced minima at the kinetic curve, it is necessary to assume that the minima are connected to the process of center transformation in the holographic planes. Probably, there is a variety of color center types in the formatted holographic planes; however, the distribution of these types varies with time (exposure) in accord with a scheme as follows: simple → long-wavelength quasi-colloidal → short-wavelength quasi-colloidal → colloidal centers. In the process of this conversion, the mass center of the absorption bands crosses twice the readout wavelength when moving to the larger wavelengths and backward. The points of these crossing correspond, according to Kramers-Kronig relation

$$\delta n(\nu_1) = \frac{c_0}{2\pi^2} \int_0^\infty \frac{\delta\alpha(\nu)\, d\nu}{\nu^2 - \nu_1^2} \tag{1}$$

(where c_0 is the light speed in vacuum, $\delta n(\nu)$ and $\delta\alpha(\nu)$ are the modulations of the refractive index and absorption coefficient, respectively), to the second and the third minima. In these points, the hologram is a purely amplitude one.

One should note that the above scheme of center transformation shows only a general trend rather than the details of this process. Actually, there are several types of color centers/electron traps in the holographic planes. Electrons released from these traps and anion vacancies recombine with both the formation of *F*-centers and complication of the existing center structures. The recombination can occur on the colloidal centers with an increase in their size. Simultaneously, the colloidal centers decay with the formation of quasi-colloidal, in particular, short-wavelength quasi-colloidal centers, that absorb at the readout wavelength. This consideration explains the amplitude nature of the hologram in the second minimum.

When passing the third maximum, the hologram has the amplitude-phase nature. At the third minimum, the hologram becomes the amplitude one again because of overlapping the readout wavelength with the quasi-colloidal absorption bands.

After passing the third minimum, the hologram is gradually converted from the amplitude-phase into the predominantly phase one and its DE increases. Some decrease in DE after ~80000 seconds down to a certain saturation value is connected to the short-wavelength quasi-colloid → colloid transformation (moving away the absorption band from the readout wavelength).

5. Hologram profile

Due to the diffusion-drift recording mechanism, the hologram profile does not reproduce the sinusoidal distribution of light intensity in the fringe pattern. The flows of electrons and vacancies off their maxima to minima result in the compression of holographic planes. As a result, several diffraction orders are observed. Below, the profile of a hologram recorded by 532 nm laser with a moderate DE of ~10% in the first order (the readout wavelength being the same) is discussed [13].

Figure 7 shows images of the 15 × 15 μm^2 area of this sample obtained using the confocal laser scanning microscope (LSM) in (i) the light of the crystal luminescence excited by argon ion laser operating at 514.5 nm and (ii) the transmitted excitation light. The luminescence is due to M and M_A^+ color centers (the M_A^+-center is the M-center in which the Na^+ ion present in the crystal as a trace impurity is incorporated). The transversal profiles of the grating obtained from the images shown in **Figure 7** are presented in **Figure 8**. The transmittance profile is close to the sine curve, whereas the luminescence profile deviates substantially from this shape.

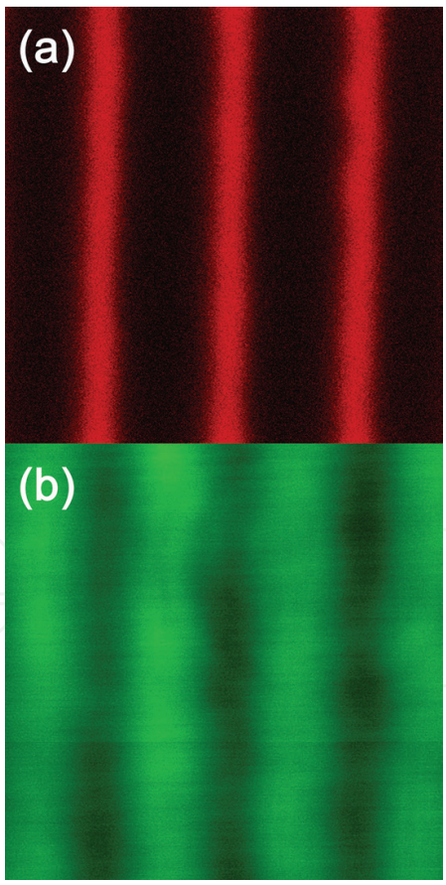

Figure 7. Images of the 15 μm × 15 μm area of the sample with a holographic grating obtained using confocal LSM: (a) in the light of the crystal luminescence excited by an argon ion laser operating at 514.5 nm and (b) in the transmitted excitation light.

http://dx.doi.org/10.5772/66114

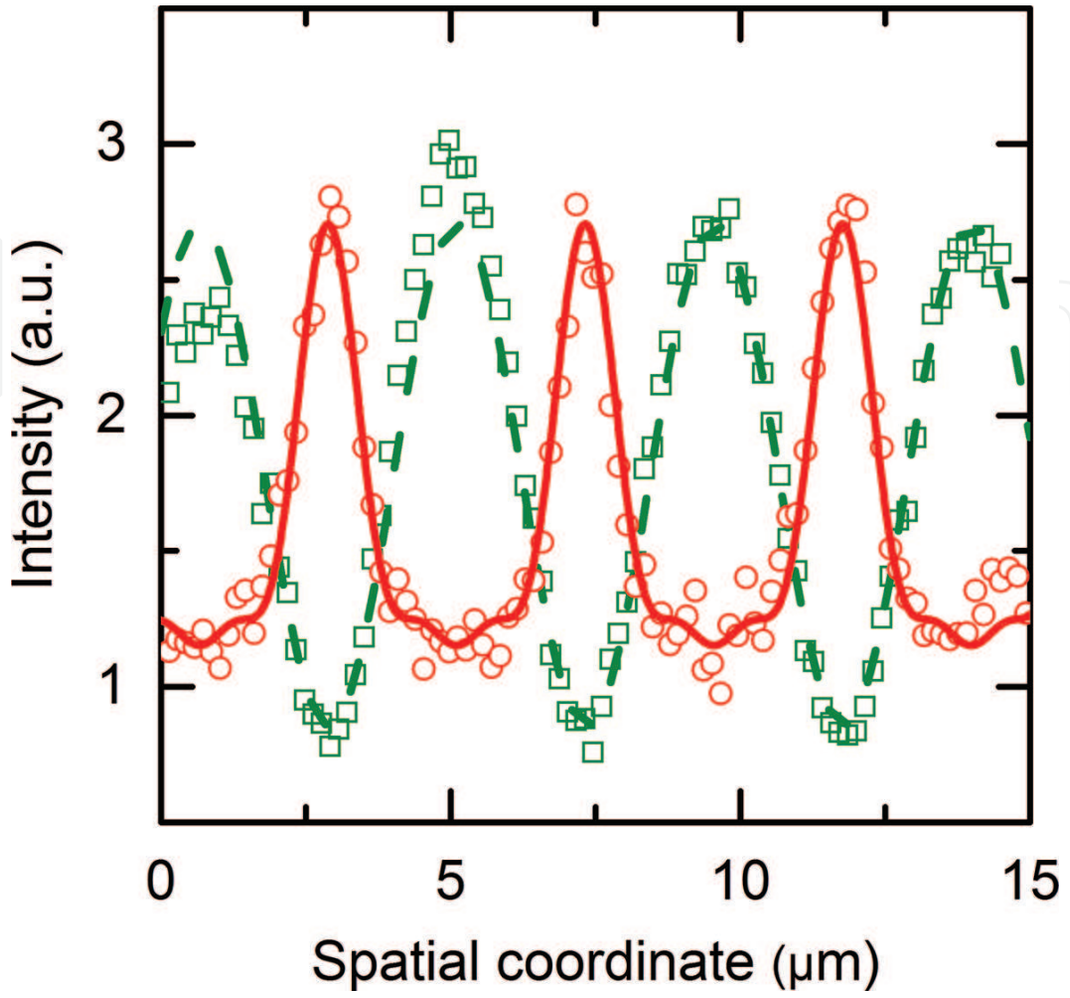

Figure 8. Transversal profiles of the grating obtained from the images shown in **Figure 7**: the transmittance profile (squares) and its sine-approximation (dashed curve); the luminescence profile (circles) and its best fit with the sum of the first three harmonic components, the amplitude ratio being 100:50:19 (solid curve).

Due to spatial filtering of optical signals with the pinhole diaphragm, confocal microscopy provides enhanced selectivity and contrast of fluorescent and reflection images: only light emitted (or scattered) within a tiny focal volume is collected at the photodetector. 3D images are constructed of "optical slices" obtained by layer-by-layer scanning of an object at different focal positions. Contrastingly, the transmitted-light images of the same thin layers include signal coming from the light cone passing through entire thickness of the sample, and the major contribution to the resulting picture is given by a number of defocused images of hologram sections. Summation of such patterns results in a nearly sinusoidal distribution, even if the original grating consisted of sharp thin lines.

Higher diffraction orders of a volume holographic grating observed at the Bragg angles θ_m corresponding to spatial frequencies $K_m = 2\pi m/d$, where d is the spatial period of the pattern, imply its nonsinusoidal shape. In order to reconstruct the spatial dependences of the refractive index $n(x)$ and absorption coefficient $\alpha(x)$ of the grating (spatial profiles), we apply partial

Fourier series with harmonic coefficients δn_m and $\delta \alpha_m$ obtained from measured angular dependences of diffraction efficiencies for respective orders and alternating signs by analogy with Fourier expansion of the truncated cosine function:

$$\delta n(x) = \sum_m (-1)^{m+1} \delta n_m \cos\left(\frac{2\pi m x}{d}\right), \tag{2}$$

$$\delta \alpha(x) = \sum_m (-1)^{m+1} \delta \alpha_m \cos\left(\frac{2\pi m x}{d}\right) \tag{3}$$

Here, x is the spatial coordinate along the grating vector K.

To determine the values of harmonic components, the angular dependences of the hologram response for three (most intense) diffraction orders can be used. The angular dependences of the zeroth and ±1st diffraction orders read out at $\lambda = 532$ nm are symmetric with respect to the normal incidence as well as those of the higher diffraction orders (**Figure 9**).

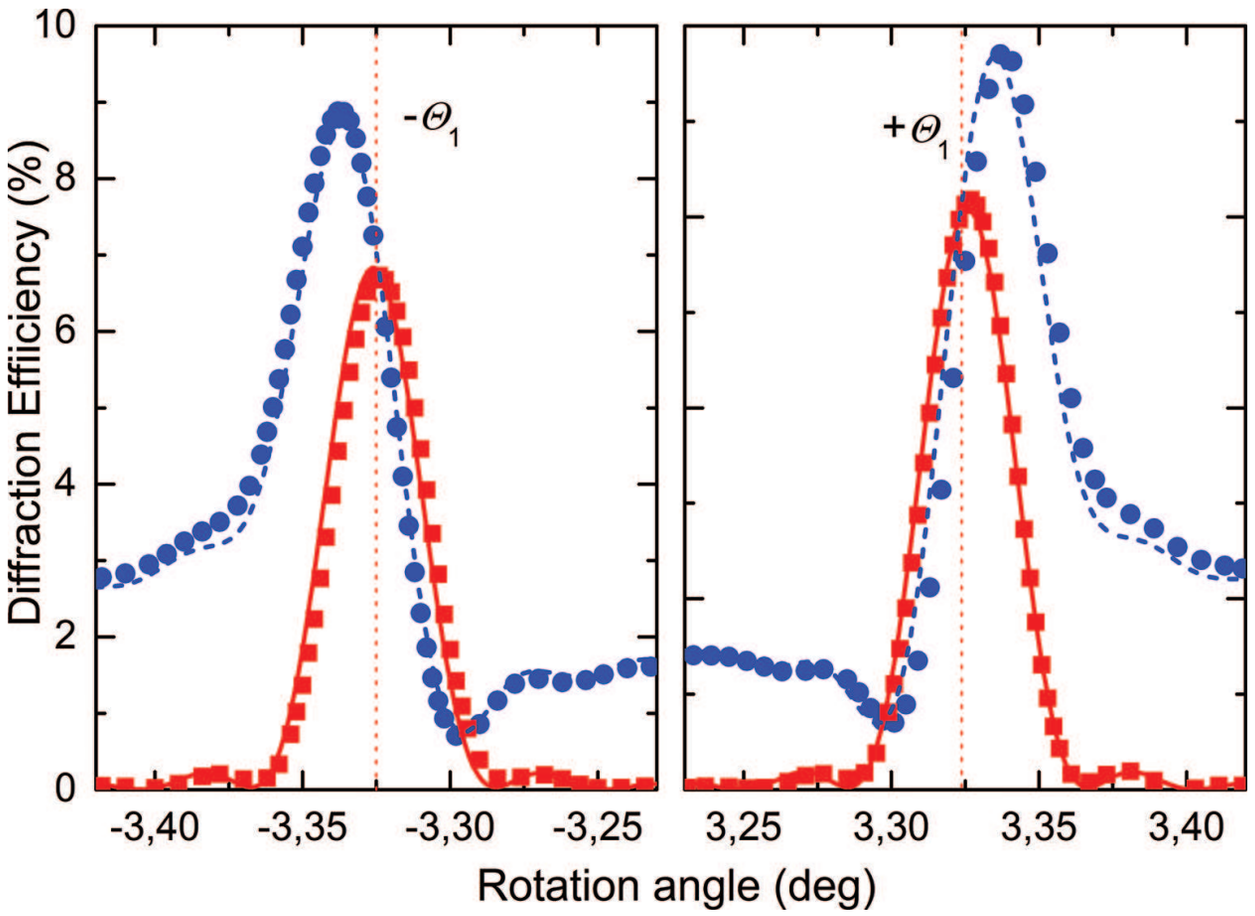

Figure 9. Angular dependences of the zeroth and ±1 diffraction orders for the grating when read out at 532 nm. Circles (η_0) and squares ($\eta_{\pm 1}$) are referred to the experimental data; dashed, and solid curves correspond to the theoretical approximation using Eqs. (5) and (4), respectively.

Using a criterion given in Refs. [14, 15], namely, that of the effectively equal values of diffraction efficiencies in the +1 and -1 diffraction orders, one can conclude that the hologram has

http://dx.doi.org/10.5772/66114

an amplitude-phase nature with the amplitude and refractive index gratings being in phase. Therefore, to fit the experimental angular dependences, the following expressions can be used for the angular dependences of the diffraction efficiencies η_m, η_0 in the mth ($m \neq 0$) and zero orders.

$$\eta_m(\theta) = 2\exp\left(-\frac{2\alpha_0 t}{\cos\theta}\right)\frac{\kappa_1^2+\kappa_2^2}{z_0}\left\{\cosh\left[\frac{\sqrt{z_0}\,t\cos(\psi/2)}{\cos\theta}\right]-\cos\left[\frac{\sqrt{z_0}\,t\sin(\psi/2)}{\cos\theta}\right]\right\}, \tag{4}$$

$$\eta_0(\theta) = \frac{\exp\left(-\frac{2\alpha t}{\cos\theta}\right)}{z_0}\left\{\begin{array}{l}\frac{\vartheta^2+z_0}{2}\cosh\left[\frac{\sqrt{z_0}\,t\cos(\psi/2)}{\cos\theta}\right]-\frac{\vartheta^2-z_0}{2}\cos\left[\frac{\sqrt{z_0}\,t\sin(\psi/2)}{\cos\theta}\right]\\ +\vartheta\sqrt{z_0}\sin(\psi/2)\sinh\left[\frac{\sqrt{z_0}\,t\cos(\psi/2)}{\cos\theta}\right]-\vartheta\sqrt{z_0}\cos(\psi/2)\sin\left[\frac{\sqrt{z_0}\,t\sin(\psi/2)}{\cos\theta}\right]\end{array}\right\} \tag{5}$$

Here $\alpha_0 = 3.29$ cm^{-1} is the mean absorption coefficient of the crystal at readout wavelength, $n_0 = 1.43$ is its mean refractive index, t is the thickness of the grating in n_m, and α_m are the modulation amplitudes of the mth harmonics of the refractive index and absorption coefficients, $\kappa_1 = \pi n_m/\lambda$, $\kappa_2 = \alpha_m/2$,

$$\vartheta = \frac{4\pi n_0 \sin\theta_m}{\lambda}(\sin\theta - \sin\theta_m), \tag{6}$$

$$z_0 = \left[(\vartheta^2 + 4(\kappa_1^2 - \kappa_2^2))^2 + (8\kappa_1\kappa_2)^2\right]^{1/2}, \tag{7}$$

$$\psi_0 = \operatorname{acos}\left\{-\frac{[\vartheta^2 + 4(\kappa_1^2 - \kappa_2^2)]}{z_0}\right\} \tag{8}$$

Modulation amplitudes for the mth harmonics of the absorption coefficient and refractive index found as the fit parameters are shown in **Table 1**.

Using data given in the second and third columns of **Table 1**, one may determine the ratios of amplitudes for the first three harmonic components of the hologram. These ratios are 100:58:22 and 100:42:14 for the absorption coefficient and refractive index, respectively. A difference between the ratios is probably caused by the presence of several types of color centers in the crystal and disproportionality of the spatial distributions of different type centers along the grating vector. Accordingly, the relative magnitudes of modulation amplitudes of the absorption coefficient and refractive index for different spatial harmonics appear to be similar but unequal.

Harmonic number	Modulation amplitude of the absorption coefficient, $\delta\alpha_m$ (cm^{-1})	Modulation amplitude of the refractive index, δn_m
1	2.13	2.6×10^{-5}
2	1.24	1.1×10^{-5}
3	0.47	0.36×10^{-5}

Table 1. Grating parameters.

The hologram profile determined from the luminescence measurements (i.e., the spatial distribution of luminescent color centers) is adequately described by the sum of three harmonic components (amplitude ratio 100:50:19, **Figure 8**). This ratio does not differ strongly from the harmonics ratio for the absorption profile 100:58:22 that follows from the angular dependences of diffraction efficiency and represents the spatial distribution of all color centers forming the grating. This confirms that both the spatial profiles reconstructed from holographic and microscopic measurements are determined by the same spatial distribution of color centers.

The modulation amplitude of absorption coefficient found from the analysis of angular dependences shows that the concentration of colored centers between the holographic planes is small as compared to the average absorption of the crystal with the hologram. At the saturation value of DE, this concentration does not exceed several percents of the total amount of the centers. The overwhelming majority of color centers present in the crystal with hologram are located in the holographic planes.

6. Hologram convertibility under the photothermal treatment using the incoherent radiation

The small amount of color centers (electron traps) between the holographic planes is a premise for the hologram stability with respect to the optical radiation and temperature. When the crystal with hologram is illuminated by incoherent radiation, most of the photoionized electrons arising in the holographic planes cannot be captured by these centers and be localized between the holographic planes. They return to the planes under the effect of electric field generated by their removal from centers subjected to the ionization. However, if the optical radiation is resonant with respect to the color centers dominating in the planes, the recombination of returning electrons with photoionized centers results in the formation of other centers, the type of these centers depending on the crystal temperature. This process opens up a unique possibility for the hologram reconstruction with the incoherent radiation [16, 17].

In **Figure 10**, the absorption spectra of additively colored CaF_2 crystal and sample cut of this crystal with hologram (Hologram *1*) are shown. One may see that hologram recording leads to increased absorption of colloidal centers (the shoulder at ~600 nm) at the expense of simple centers. This sample was subjected to the series of successive photothermal transformations that converted Hologram *1* to Holograms *2*–*5* (**Table 2**). The spectra of the samples with these holograms are shown in **Figure 11**. All holograms were read out using the DPSS laser (532 nm), and Holograms *2*–*5* were also read out with diode Thorlabs S3FC1550 laser (1.55 μm). The types of holograms and their DE values are shown in **Table 2**.

As seen (**Figure 12**), noticeable narrowing of the profile of the treated holograms and an accompanying increase in the intensity of the higher diffraction orders occur.

These facts can be explained by spatial redistribution of various center types in Hologram *1*. The highly aggregated color centers are located predominantly in the immediate vicinity of the

http://dx.doi.org/10.5772/66114

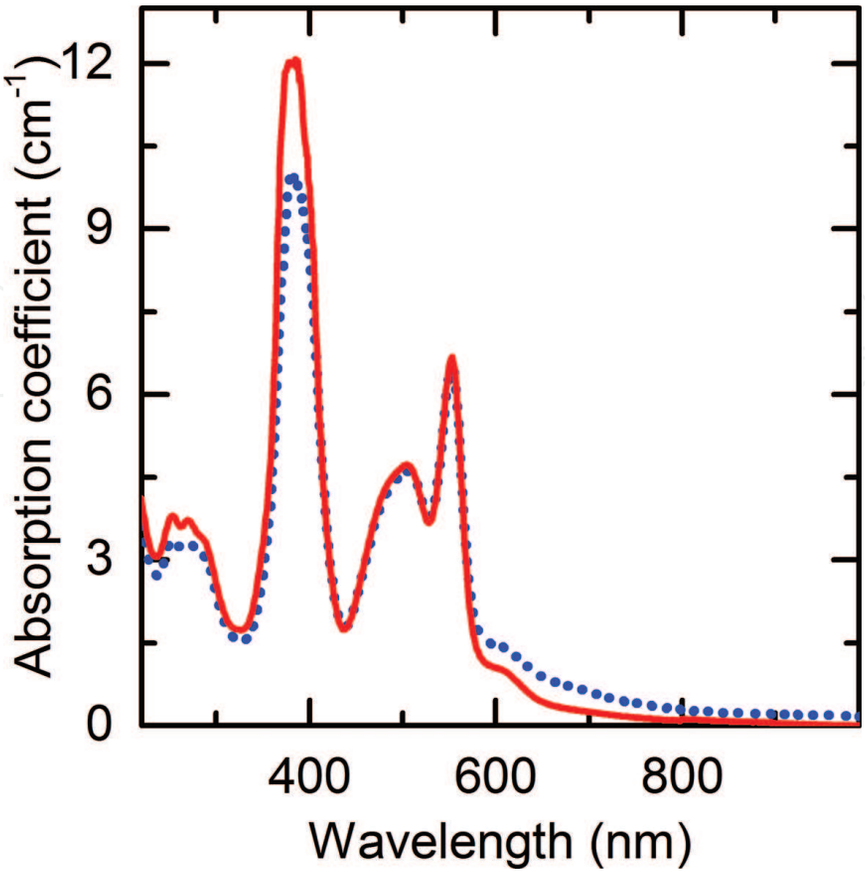

Figure 10. Absorption spectra of CaF_2 sample with color centers before (solid line) and after (dotted line) recording Hologram *1*.

Stage of treatment	Hologram number	T (°C)	Impact λ (μm)	Impact time (h)	Exposure (kJ cm^{-2})	Hologram type at 532 nm readout	+1st order DE at 532 nm readout	Hologram type at 1.55 μm readout	+1st order DE at 1.55 μm readout
Hologram recording	1	-	-	-		Amplitude-phase (in-phase)	7.8	Not measured	-
(1)	2	82	0.365	36.8	10	Phase	26.0	Amplitude-phase (antiphase)	6.0
(2)	3	202 190	- >1	84.4 24.4	- 1	- Amplitude-phase (antiphase)	- 12.0	- Amplitude-phase (in-phase)	- 29.0
(3)	4	186	0.578	49.3	10	Amplitude-phase (in-phase)	6.5	Phase	4.2
(4)	5	193	0.365	6.0	1	Amplitude	14.1	Phase	14.2

Table 2. Sample treatment parameters and hologram characteristics.

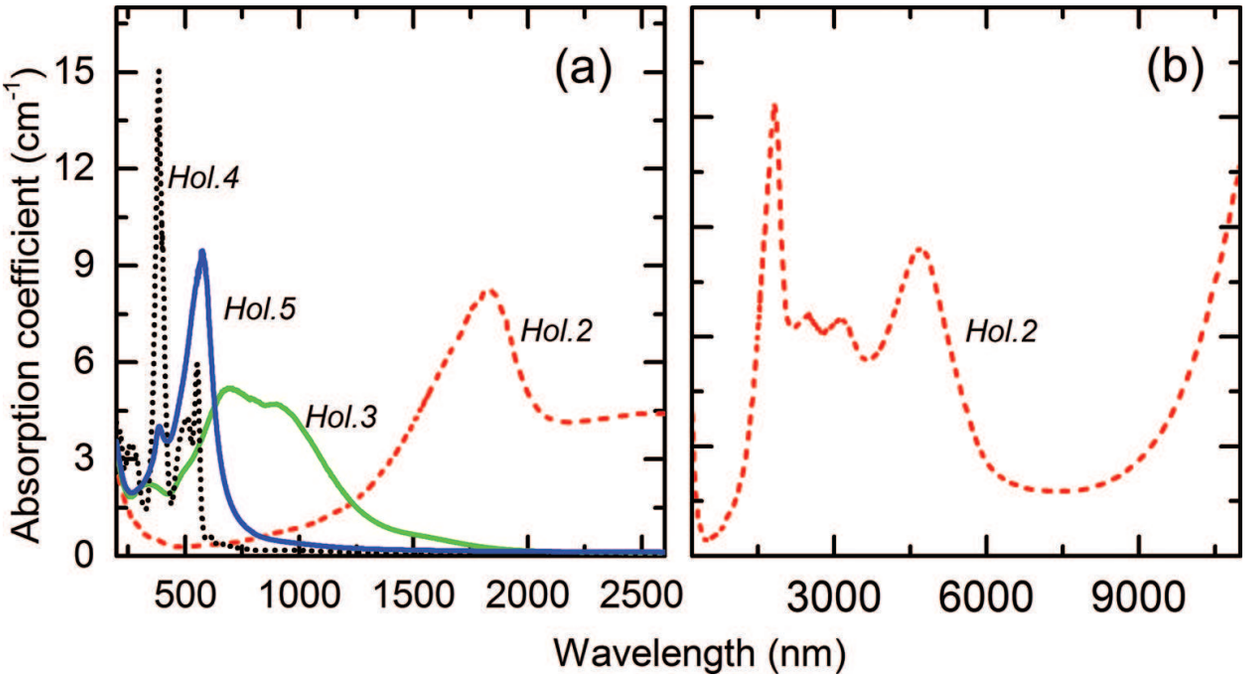

Figure 11. Absorption spectra of samples with Holograms *2*–*5* (a) and Hologram *2* in the extended wavelength range (b).

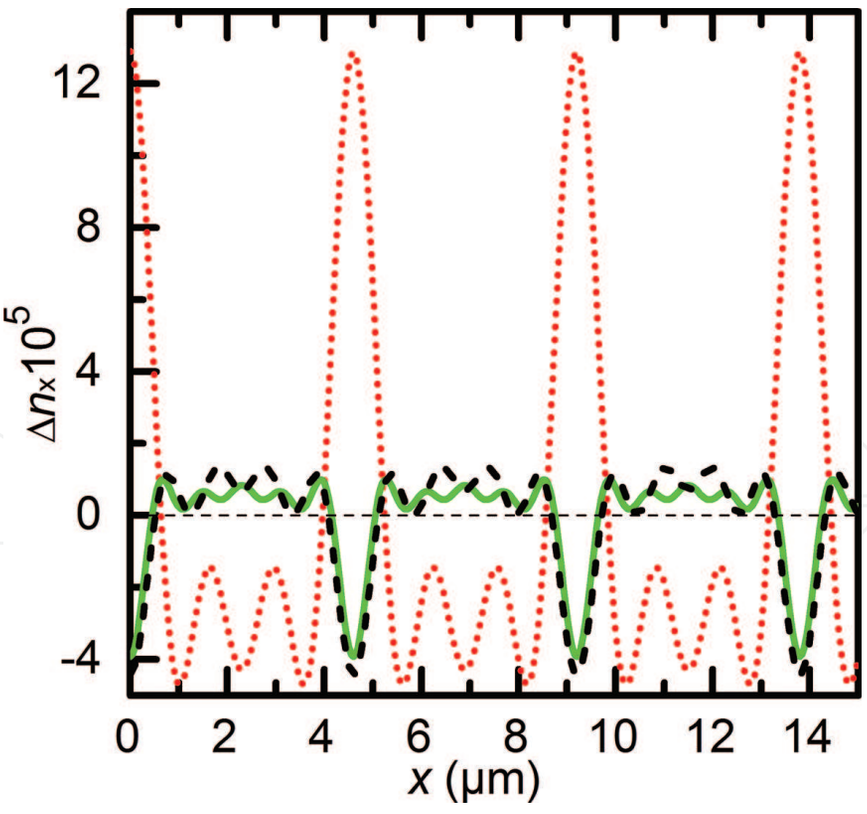

Figure 12. Refractive index profiles of Hologram *1* (dotted line), Hologram *2* (solid line), and Hologram *3* (dashed line) as reconstructed from the angular dependences of the diffraction response at 532 nm. The half-widths of the profiles are 1.00 μm (Hologram *1*), 0.65 μm (Hologram *2*), and 0.70 μm (Hologram *3*).

http://dx.doi.org/10.5772/66114

fringe pattern minima, where the density of vacancies/electrons is relatively high, whereas the peripheral areas of these minima contain mainly simple centers. During Stage (1), the 365 nm radiation effectively destroys the simple centers because all of them have the absorption bands located near this wavelength. However, this radiation just weakly affects the highly aggregated centers. Electrons arising under the photoionization of simple centers move towards the central areas of holographic planes, where the concentration of color centers (traps) is higher than that at the peripheral areas and localize there generating an electric field that attracts vacancies. This increases somewhat the center concentration in the central areas and forms the quasi-colloidal centers stable at temperature of about 80°C. This results in narrowing the Hologram *2* profile that becomes more meander-like. As shown in **Figure 11**, the transformation of the long-wavelength quasi-colloidal centers into the predominantly short-wavelength quasi-colloidal and colloidal ones does not result in a noticeable change of the profile. It should be noted that, at elevated temperatures, the color centers of various types are in equilibrium with each other. The equilibrium state can shift toward a certain type of color centers depending on temperature and, on illuminating the sample, on the wavelength and intensity of the light. At Stages (1) and (2), both heating and the illumination play the same role in facilitating the concentration of the centers and their transforming into the long-wavelength quasi-colloidal centers during Stage (1) and into the short-wavelength and colloidal centers during Stage (2); this is the reason for narrowing the profiles of Holograms *2* and *3*. During Stage (3), in contrast, these factors act in the opposite directions. The temperature of 186°C favors the colloidal center formation; however, the 578 nm radiation destroys them, as well as the short-wavelength quasi-colloidal centers present in Hologram *3*, thus hindering the accumulation of color centers, which results in some broadening the Hologram *4* profile.

The sample with the hologram under above transformations was maintained at 80–190°C for more than 8 days and ~2/3 of this period the sample was under the impact of actinic radiation with the total exposure of 22 kJ cm^{-2}. Such treatment does not result in the hologram erasure. It should be noted that (i) the absorption spectrum of the sample with Hologram *4* thus treated practically coincides with the spectrum of the initial sample and (ii) DE of the hologram is reduced only by ~1.3% as compared to that of Hologram *1* (it should be taken into account that these two holograms are similar but not wholly identical). As seen, one can state an extremely high stability of holograms in this medium with respect to the optical radiation and temperature.

The read out of Hologram *5* with 532 nm laser shows the equality of intensities of diffracted and transmitted radiation (Borrmann effect) due to a large absorption at the readout wavelength.

The above considerations allow for managing the hologram type (amplitude-phase, mostly amplitude, or mostly phase one), characteristics, and diffraction efficiency. Such changes can be implemented throughout the visible and IR spectral ranges up to the CaF_2 transparency limit (10 μm). It should be noted that **Figure 11** shows only the examples of center-type transformation. Actually, one can perform the finer "tuning" of the center type by modifying the wavelength of incoherent radiation and temperature. The other ruling parameter is the concentration of color centers in the crystal (the additive coloring mode).

7. Self-organization of color centers in the course of hologram recording

The investigation of weakly colored samples with holograms recorded under various power densities of laser radiation, exposure, temperature, and grating period revealed structuring the holographic planes with an increase in the colloidal center concentration: the holographic planes became thinner and were pierced by fragmentary spiral-like bundles that consisted of colloids.

Figure 13 shows the 3D view of such hologram composed with the confocal LSM. One may conclude that, under hologram recording, (i) the above self-organization of color centers took place and (ii) the colloidal centers played an important role in this process [18, 19].

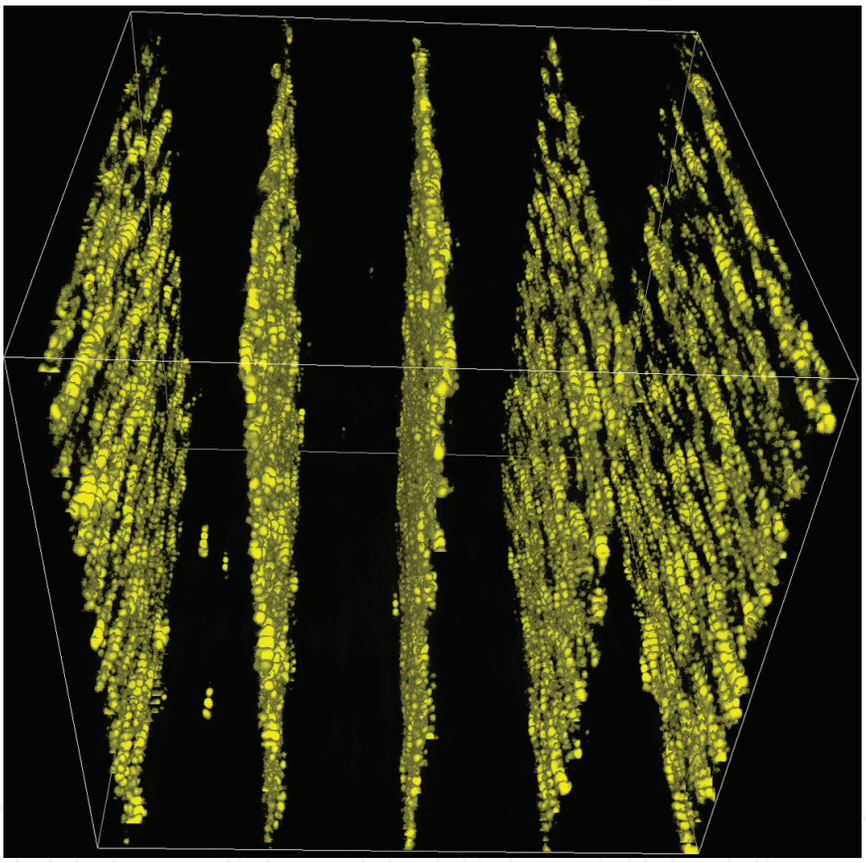

Figure 13. 3D LSM image of the sample with bundles in the holographic planes seen in the reflected light of 405 nm laser.

The colloidal particles can be considered as the second phase inclusions in the fluorite lattice. It should be noted that, though metallic calcium and fluorite have the same Bravais lattice and mismatch of their lattice parameter, a, is very small ($a_{Ca} = 0.556$ nm, $a_{CaF_2} = 0.545$ nm), the mutual orientation of the matrix and colloids is not expected to be cube-on-cube [5]. Thus, the colloidal centers disturb the fluorite lattice. This disturbance displays itself in broadening the absorption bands with the growth of the colloid content.

It was stated above that the color centers including colloids both form and decay in the hologram recording process. So, recording a hologram on the CaF_2 crystals with color centers is accompanied by continuous phase transitions.

http://dx.doi.org/10.5772/66114

The internal self-consistency (self-organization) arises in complex systems due to the interaction of various subsystems [20]. Their interaction is the most effective near the phase transition; when a subsystem that experiences the transition becomes soft and weak, an external perturbation can cause the strong modification of the subsystem state and, in particular, its order parameter. In the case under consideration, such perturbations could be the fluctuations of concentrations of simple centers, vacancies, and electrons. These fluctuations could, in turn, trigger the formation of large-scale stable spatially inhomogeneous states in the subsystem of colloidal centers located in the holographic planes. Such states are bundles. The bundles arise in the recording conditions and turn out to be frozen on cooling the crystal after finishing the recording process.

The bundle formation is probably governed by (i) bi-directional "compression" of holographic planes by vacancy flows emanating from the neighboring fringe pattern maxima (the bundle thickness is about the thickness of the holographic planes) and (ii) the direction of the Poynting vector of the interference field that determines successive recording of the hologram deeply into the sample (the bundle orientation coincides with this direction).

Within the framework of the synergetic theory [20], a CaF_2 crystal in the process of hologram recording may be considered as an open system that is in the heat exchange with a heat source having temperature of 150–200°C. From this standpoint, the formation of bundles (dissipative structures) is the result of importing the negative entropy into the crystal.

At some colloid content, the bundles become continuous and correlated with each other, thus forming the 2D superlattice of a symmetry very close to *cmm* plane symmetry group [21] with the lattice parameters as follows: a is the doubled period of the hologram and b is a separation between the neighboring bundles along the holographic plane (**Figure 14**). For the sample shown in **Figure 13**, $a = 9$ μm and $b \approx 4.2$ μm. Under further increase in the colloid concentration, however, the correlation between bundles breaks and they tear off.

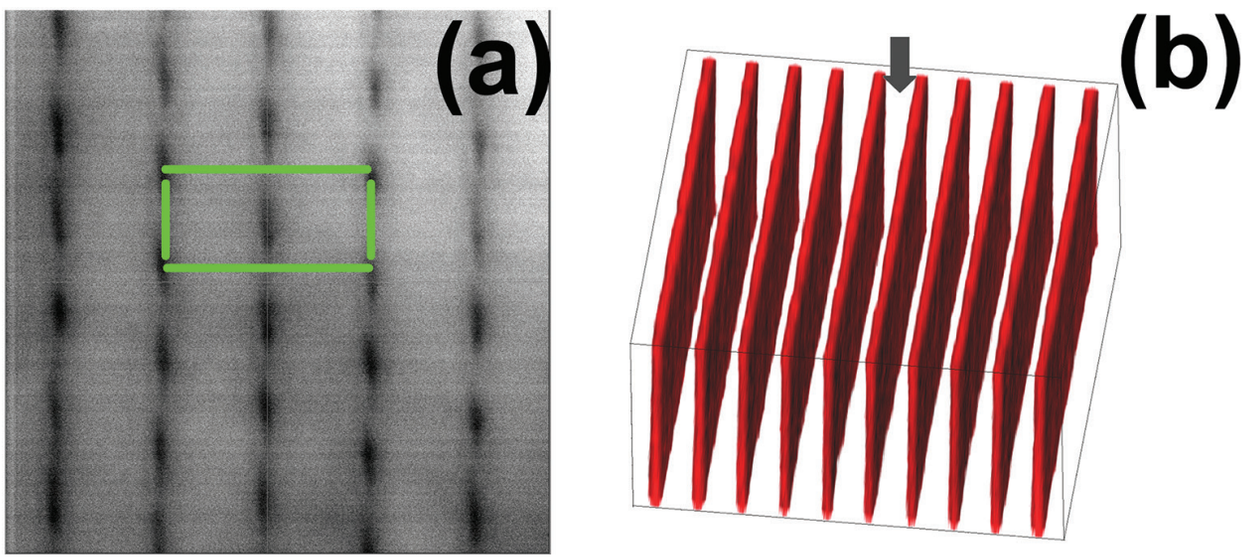

Figure 14. Absorption image of a hologram with 2D superlattice in one of orthogonal projections resulted from postprocessed series of their optical slices recorded using LSM at 405 nm (a). The schematic drawing of hologram (b); an arrow indicates the projection shown in (a). The green rectangle in (a) shows the superlattice elementary cell.

Earlier, the colloid cubic superlattice with the lattice parameter of ~20 nm was observed on the surface of electron-irradiated crystals (see [22] and references therein).

8. Possible applications of the holograms

The main characteristic features of holograms on CaF_2 crystals with color centers are as follows: (1) the opportunity of preparing thick holograms with high angular and spectral selectivities, (2) an extremely high hologram stability with respect to the effects of optical radiation and temperature, and (3) an opportunity to transform the composition of color centers forming the holographic grating via the postexposition photothermal treatment, i.e., to change the type of hologram at the desired readout wavelength. The volume holographic elements with such features and spatial resolution of about 5000 lines mm^{-1} and more can be useful for solving many problems. Below, two possible applications of such elements are discussed.

8.1. Plane angle measure

A conventional plane-angle measure is a regular polyhedral-fused silica prism, whose angles are set by normals to its faces. Each normal is implemented physically by the autocollimator axis when the cross hairs in its focal plane are aligned with the image arising as a result of collimated beam reflection from the prism face. The angle between two normals is reproduced by rotating the prism around an axis perpendicular to the autocollimator measuring plane. Thus, the set of angles stored by the prism is determined by the mutual positions of its faces and is reproduced using the light beam reflected from them and sample rotation. The prism reproduces angles with effective values close to $m(360/n)°$, where n is the number of lateral faces and $m = 1, 2, \ldots, n - 1$ (actually, $n \leq 72$). Such a fused silica prism has drawbacks as follows: a large weight and size (1.2 kg and more, dimensions 170 × 20 mm and more); the discreteness of the formed plane angle circular scale that is limited by the number of faces (up to 36 faces); a low production efficiency (the prism preparation is, in principle, the custom-made, time-consuming process); and the hazard of spontaneous sharp changes, when storing, in the optical and geometric characteristics (so-called devitrification).

A new multivalued plane-angle measure based on the holographic principle that has a number of significant advantages over the fused silica prism was proposed [23–26].

This element (referred to below as sample) is a parallelepiped made of a photochromic CaF_2 crystal in which a system of superimposed holograms is recorded. Their mutual spatial positions form a set of angles (the multivalued holographic measure) stored by this element. The exposure of this sample to a reference laser beam induces a response in the form of several diffracted beams. Depending on the recording method, they arise successively or simultaneously upon rotating the sample and cover a limited range of angles; these beams are recorded by photoelectric detector. The rotation of the sample makes it possible to form a full angular scale.

Angles between directions set by the holograms are the functional analogs of angles between the fused silica prism normals. Hence, this element can be referred to as a holographic prism,

http://dx.doi.org/10.5772/66114

HP. For this prism, an angle between holograms forming it can be fairly small (of the order of an arc minute). This circumstance provides a high discreteness of the realized circular scale and, correspondingly, high accuracy of angular measurements.

A holographic prism, as noted above, can be implemented in two modifications, I and II, that produce the set of angles. For modification I, the temperature-controlled housing with a sample is mounted on the rotation table, their rotation axes coinciding. The interfering beams are in the plane parallel to the table. After recording the first hologram, the sample is turned by the assigned angle to record the next hologram, and so on. Several superimposed holograms form HP-I. Then, the sample is mounted on the rotation stage and the diffraction responses of the holograms appear successively when rotating the table (**Figure 15**) [23]. The half width of angular selectivity profile of a 14 × 8.5 × 7.7 mm sample with the hologram thickness of 8.5 mm is 1.8′.

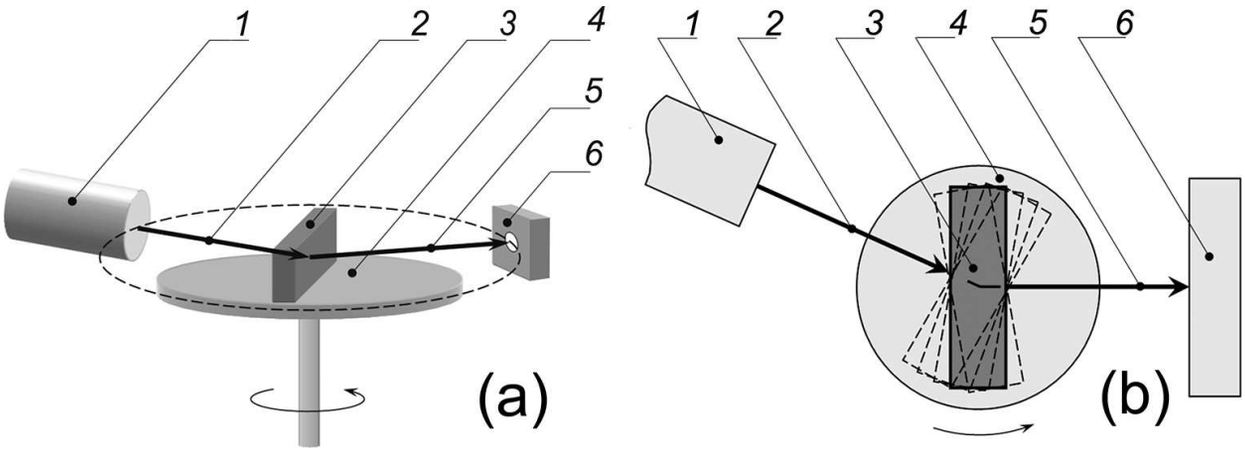

Figure 15. General view (a) and top view (b) of HP-I holographic prism: (*1*) is the reference laser, (*2*) is the incident beam, (*3*) is the holographic prism, (*4*) is the rotation stage, (*5*) is the diffracted beam, and (*6*) is the photodetector.

To record an HP-II, one should use an interferometer wherein the coherent beams cross each other at an angle of 90°. A sample is installed in their interference region on the table of the rotational device. The first beam is aligned with the device axis, whereas the second one, as indicated above, is perpendicular to the first beam. The system of holograms forming HP-II is recorded successively, and the crystal is rotated by a specified angle after each recording cycle. Holograms thus recorded can be reconstructed simultaneously by the same reference beam that has a direction the same as the first recording beam. The diffracted (signal) beams are oriented perpendicularly to the reference beam. Angles between the beams are the angles of crystal rotation in the course of prism recording. This method for recording the imposed holograms can be used to implement on condition that they are recorded and reconstructed by radiation with the same wavelength, so that the angle of beam convergence specified at recording is exactly reproduced during the reconstruction. The fan of diffracted beams emitted by HP-II and the reference beam are shown in **Figure 16** [25]. Holograms were reconstructed with the reference beam of ~1 mm in diameter that is much smaller than the hologram diameter (~8 mm); so, the diffracted beams formed extended enough lines on the screen.

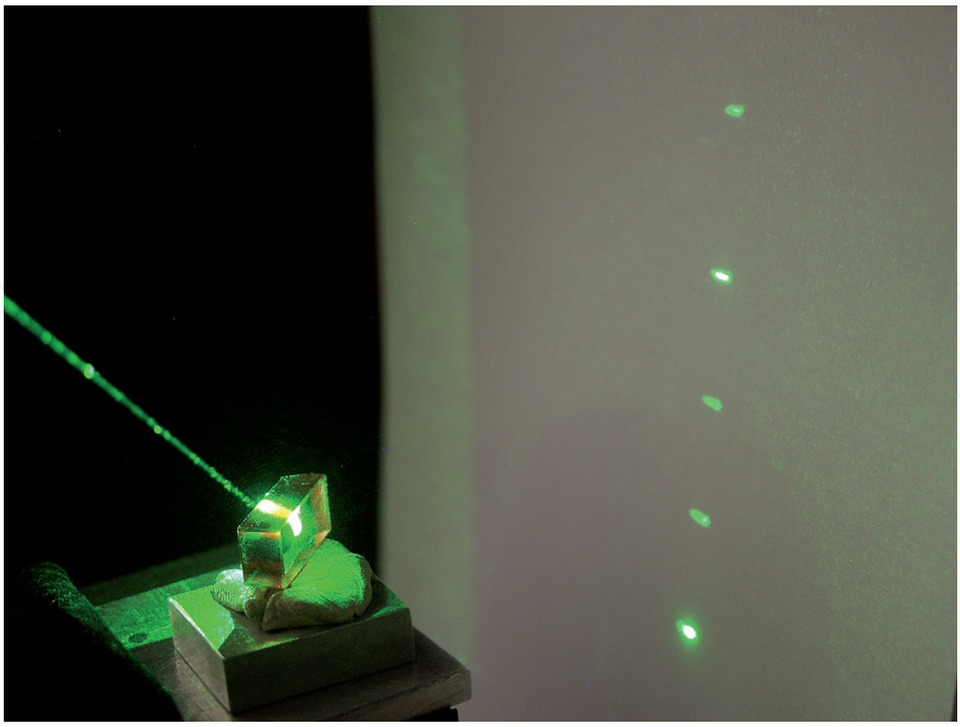

Figure 16. Fan of diffracted beams emerging from HP-II.

The uniquely small mass and dimensional characteristics of this angular measure (10 g and 0.5–1 cm^3, respectively) make it possible to use such HP as a basis for developing devices for measuring/setting rotation angles that will combine two antinomic requirements such as the mobility and high accuracy of angular measurements (see [25] for details).

8.2. Volume holographic elements for mid-IR spectral range

The specific features of holograms listed above allow for taking the holographic elements based on additively colored CaF_2 crystals to be quite promising as the transmission and reflection filters in the mid-IR spectral range. Below, the expected characteristics of holographic filters based on CaF_2 crystals with photothermally transformed holograms are discussed.

The absorption spectrum of CaF_2 crystal after special photothermal treatment is shown in **Figure 17**. An absorption band attributed to the short-wavelength quasi-colloidal centers ($\lambda_{max} \cong 2$ μm) is present in the spectrum.

Under suggestions that (a) the absorption spectrum of the sample with a hologram is similar to that shown in **Figure 17**, (b) the holographic grating plane width is about 0.2 of the grating period d (e.g., 1 μm width at 4.5 μm period [13]), and (c) ~90% of color centers are located within the holographic planes (and, hence, the same fraction of the sample absorption originates from the planes), it is possible to estimate the expected characteristics of transmission and reflection holograms read out with 3.5 μm radiation.

The absorption spectrum shown in **Figure 17** ensures recording of efficient transmission and reflection holograms in the crystal samples of several millimeters thick. When neglecting the

http://dx.doi.org/10.5772/66114

absorption of readout radiation, it is possible to use the Kogelnik theory to calculate the phase hologram parameters [27].

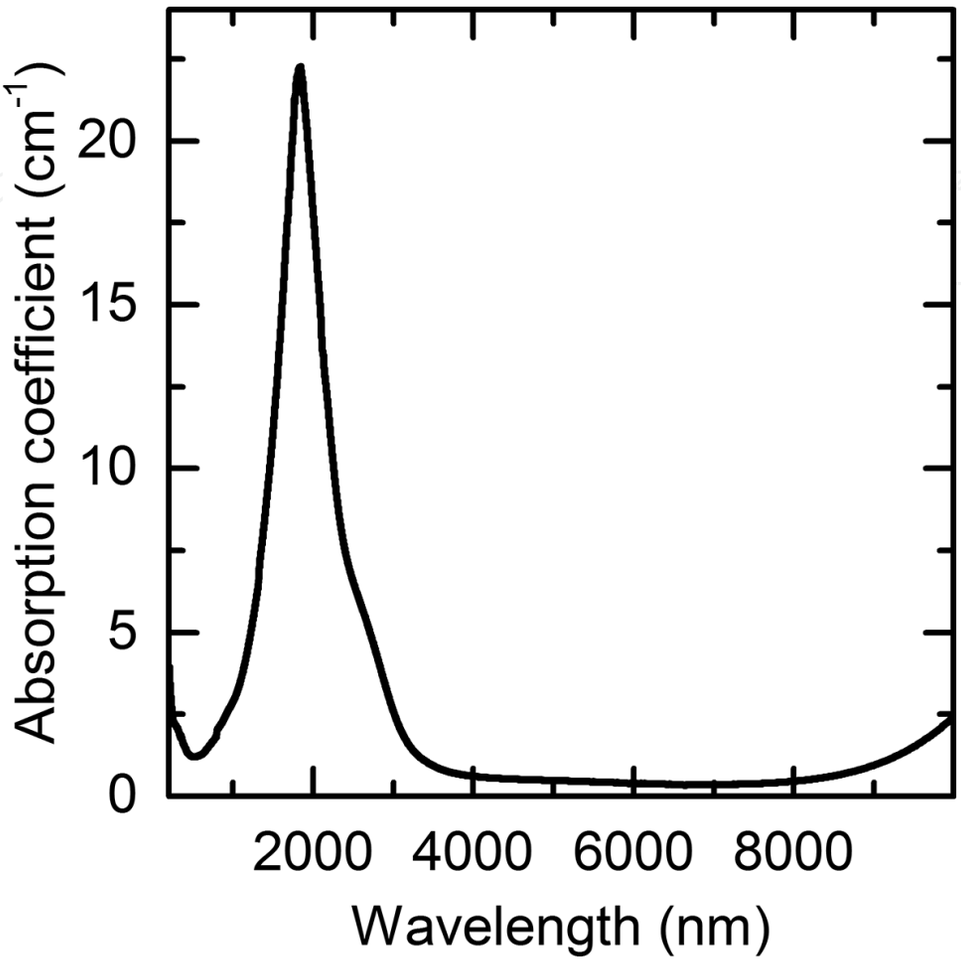

Figure 17. Absorption spectrum of the photothermally treated sample.

According to suggestions (b) and (c), the spectral dependence of the modulation amplitude of the absorption coefficient $\delta\alpha(\nu)$ of the crystal with a hologram can be calculated by multiplication of the absorption spectrum shown in **Figure 17** by coefficient such as (4.5 μm/1 μm) × 0.9. Kramers-Kronig relation (1) allows the estimation of the corresponding spectral dependence of the modulation amplitude of the refractive index $\delta n(\nu)$ shown in **Figure 18**.

The modulation amplitude of the refractive index δn at the readout wavelength λ = 3.5 μm equals to 6.82 × 10^{-4}. The hologram thickness T is determined by the phase incursion $\nu_t = \pi/2$ that provides the 100% diffraction efficiency of the phase hologram. To calculate the optimum thickness of the hologram, an expression can be used as follows:

$$T = \nu_t \lambda \cos\theta_0 / \pi\delta n, \tag{9}$$

where θ_0 is the Bragg angle for the readout radiation inside the holographic medium ($\theta_0 = 15°$ for the grating period d = 4.5 μm). The thickness of a hologram with the above parameters equals to 2.45 mm.

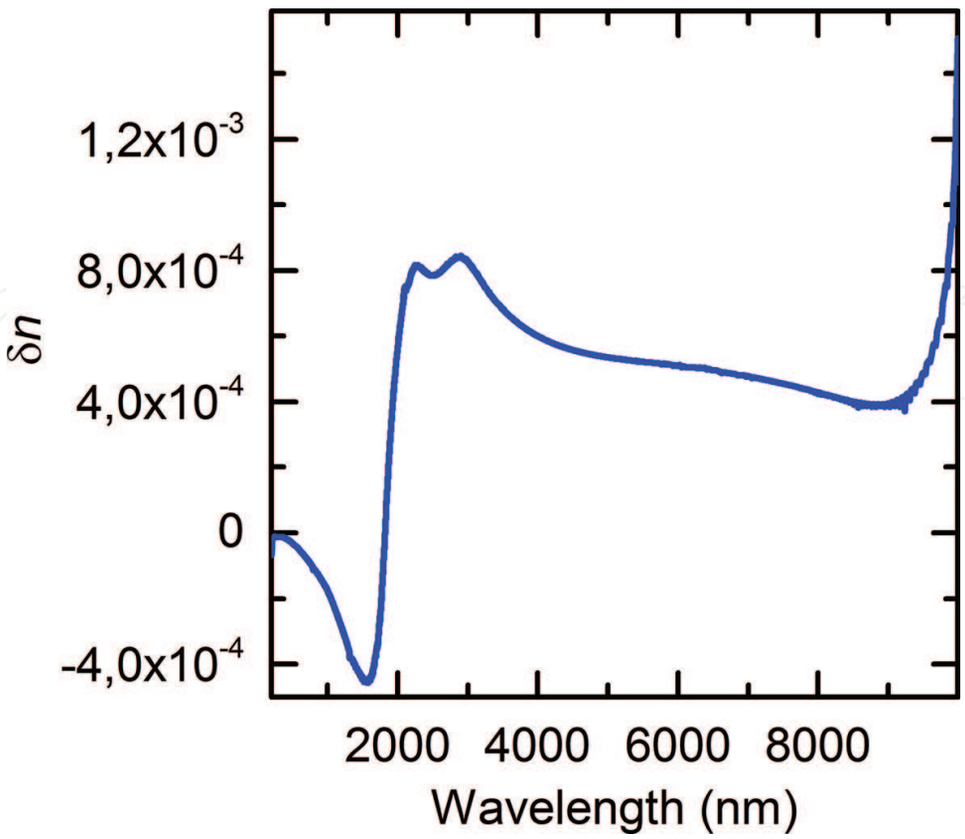

Figure 18. Spectral dependence of the modulation amplitude of the refractive index for a crystal with the hologram.

It should be noted that the nonsinusoidal nature of the hologram profile in this crystal results in the appearance of several diffraction orders from the recorded hologram (the diffraction from several spatial harmonic components). The fraction of the first diffraction order that can be used for holographic filtering at the Bragg angle is about 65% of the total diffraction efficiency of the hologram [13].

The spectral selectivity of the transmission hologram, $\delta\lambda$, can be approximately calculated using an equation as follows:

$$\delta\lambda \approx \frac{\lambda d \operatorname{ctg} \theta_0}{T} \tag{10}$$

At the above values of grating parameters, $\delta\lambda$ = 24 nm.

Angular selectivity of the hologram $\delta\theta$ is given by

$$\delta\theta = \lambda \xi_t / \left(2\pi n T \sin \theta_0\right), \tag{11}$$

where n = 1.43 is the refraction index of CaF_2 crystal at the readout wavelength. The misalignment parameter ξ_t is proportional to the deviation of the readout angle (in the medium) from θ_0. The ξ_t value of ~2.7 corresponds to DE equal to zero. Under these conditions, the angular selectivity equals to 0.13° according to Eq. (11).

http://dx.doi.org/10.5772/66114

When using the sample with hologram as a reflection-type filter, the wavelengths of recording (λ_{rec}) and reflected (λ_{read}) radiations are different but connected—according to the Bragg condition—via the hologram period d:

$$d = \frac{\lambda_{rec}}{2 \sin \theta_{rec}} = \frac{\lambda_{read}}{2 \sin \theta_{read}} \tag{12}$$

For the actual case $\theta_{read} = 90°$ at $\lambda_{read} = 3.5$ μm, the period of reflection grating d equals to 1.22 μm.

Recording of the reflection hologram readout with 3.5 μm radiation can be executed with the 532 nm radiation in the symmetric transmission scheme with the $2\theta_{rec} = 25.2°$ angle between the recording beams (**Figure 19**).

The assumption that relation between grating period and holographic plane thickness is the same for both transmission and reflection grating allows using the same $\delta n(\nu)$ dependence (**Figure 18**) to calculate the phase incursion for the reflection hologram.

The DE of the reflection hologram increases with an increase in the phase incursion, ν_r:

$$\eta = \text{th}^2(\nu_r), \tag{13}$$

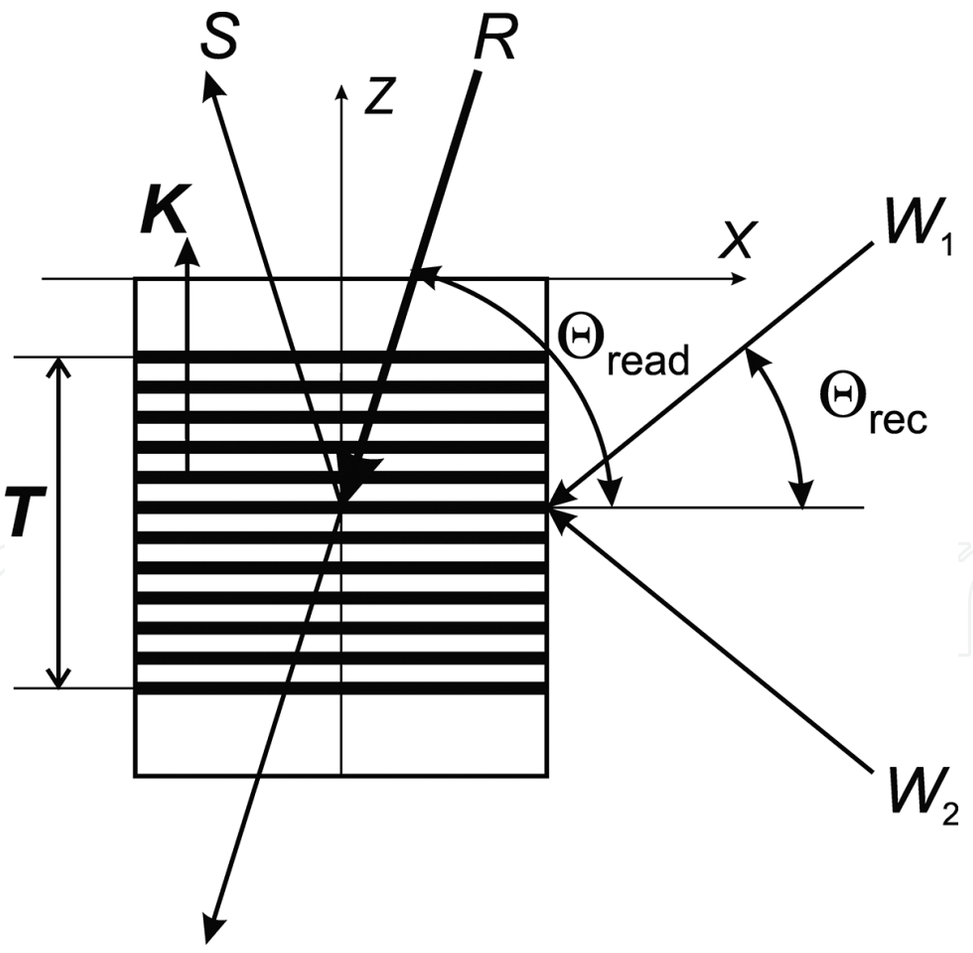

Figure 19. The scheme of recording/readout the reflection hologram. W_1 and W_2 are the recording beams, R and S are readout and diffracted beams, respectively, $K = 2\pi/d$ is the grating vector.

where $\nu_r = \frac{\pi \Delta n T}{\lambda \sin \theta_0}$. For $\delta n = 6.82 \times 10^{-4}$, the thickness of a hologram with DE = 100% equals to 6 mm. Absorption in such sample does not exceed 3%.

The spectral and angular selectivity of the reflection hologram can be expressed through the misalignment parameter ξ_r. The ξ_r value of 3.5 corresponds to the deviation of pitch angle θ_0 from its magnitude of 90°; at the latter, DE ≅ 0 and the ξ_r parameter and the spectral selectivity are connected through a relation as follows:

$$\delta\lambda = -\frac{\xi_r \lambda^2}{(2\pi n T \sin \theta_0)} \tag{14}$$

At the above ξ_r value, the spectral $|\delta\lambda|$ and angular $\delta\varphi$ selectivities are equal to 1.3 nm and 0.02°, respectively.

These estimates demonstrate the possibility of using the holographic elements based on CaF_2 crystals with color centers as the volume narrow-band transmission and reflection filters for the mid-IR spectral range.

9. Conclusions

The fluorite crystal with color centers is a promising holographic medium. The technology of its preparation allows for producing reproducibly large-size samples and enables the modification of color center concentration in a wide range. There exists the set of color centers whose absorption bands overlap with each other, thus covering the entire transparency region of fluorite. The photochromism of color centers enables hologram recording in the fluorite crystals. The diffusion-drift mechanism of recording that causes not only the color center transformation but also their redistribution over the crystal bulk determines the holographic features of this medium such as (i) the nonsinusoidal hologram profile, (ii) a high hologram stability with respect to temperature and optical radiation, and (iii) an opportunity to change the type of readout hologram (amplitude, amplitude-phase, or phase) using postexposure incoherent radiation. The highly stable volume holograms with high angular and spectral selectivities can be used as metrological elements and narrow-band transmission and reflection filters for the mid-IR spectral range.

Acknowledgements

The authors are grateful to Yurii I. Terekhin for preparing all CaF_2 samples, Tatiana S. Semenova, Lyudmila F. Koriakina, and Marina A. Petrova for additive coloring the samples, and also Evgenii B. Verkhovskii and Anatolii K. Kupchikov for a technical assistance (all of them, ITMO University).

The paper is dedicated to the memory of our colleague, Aleksandr S. Shcheulin (1955–2016), who was an active participant of this study.

Research was funded by Russian Science Foundation (Agreement #14-23-00136).

Author details

Aleksandr I. Ryskin, Aleksandr E. Angervaks* and Andrei V. Veniaminov

*Address all correspondence to: angervax@mail.ru

ITMO University, St. Petersburg, Russian Federation

References

[1] Shcheulin AS, Semenova TS, Koryakina LF, Petrova MA, Kupchikov AK, Ryskin AI. Additive coloration of crystals of calcium and cadmium fluorides. Opt. Spectrosc. 2007;**103**:660–664. DOI: 10.1134/S0030400X07100219

[2] Shcheulin AS, Semenova TS, Koryakina LF, Petrova MA, Angervaks AE, Ryskin AI. Additive coloring rate and intensity for pure and doped fluorite crystals. Opt. Spectrosc. 2011;**110**:617–623. DOI: 10.1134/S0030400X11040205

[3] Hayes W, editor. Crystals with Fluorite Structure. Electronic, Vibrational, and Defect Properties. 1st ed. Oxford: Clarendon Press; 1974. 448 p.

[4] Orera VM, Alkala E. Optical properties of cation colloidal particles in CaF_2 and SrF_2. Phys. Status Solidi. 1977;**44**:717–723. DOI: 10.1002/pssa.2210440239

[5] Cramer LP, Schubert BE, Petite PS, Langfort SC, Dickinson JT. Laser interactions with embedded Ca metal nanoparticles in single crystal CaF_2. J. Appl. Phys. 2005;**97**:074307. DOI: 10.1063/1.1862758

[6] Rix S, Natura U, Loske F, Letz M, Felser K, Reichling M. Formation of metallic colloids in CaF_2 by intense ultraviolet light. Appl. Phys. Lett. 2011;**99**:261909. DOI: 10.1063/1.3673301

[7] Shcheulin AS, Angervaks AE, Aksenova KA, Gainutdinov RV, Ryskin AI. Photothermal transformation of color centers in CaF_2 crystals. Opt. Spectrosc. 2015;**118**:542–546. DOI: 10.1134/S0030400X15040189

[8] Belous VM, Mandel VE, Popov AY, Tyurin AV. Mechanism of holographic recording based on photothermal transformation of color centers in additively colored alkali halide crystals. Opt. Spectrosc. 1999;**87**:305–310.

[9] Popov AY, Belous VM, Mandel VE, Shugailo VB, Tyurin AV. Drift model of photo-induced processes in alkali-halide crystals during hologram recording. Proc. SPIE. 1999;**3904**:195–200. DOI: 10.1117/12.370402

[10] Shcheulin AS, Veniaminov AV, Korzinin YuL, Angervaks AE, Ryskin AI. A highly stable holographic medium based on CaF_2:Na crystals with colloidal color centers: III. Properties of holograms. Opt. Spectrosc. 2007;**103**:655–659. DOI: 10.1134/S0030400X07100207

[11] Beuneu F, Vajda P. Radiation-induced defects in CaF_2: An electron-spin resonance and dielectric constant investigation. J. Appl. Phys. 1995;**78**:6989–6993. DOI: 10.1063/1.360466

[12] Vladimirov DA, Mandel' VE, Popov AY, Tyurin AV. Optimization of the recording conditions for holograms recorded in additively colored KCl crystals. Opt. Spectrosc. 2005;**1999**:137–140.

[13] Veniaminov AV, Shcheulin AS, Angervaks AE, Ryskin AI. Profile of a volume hologram in CaF_2 crystal with color centers as determined with using confocal scanning microscopy. J. Opt. Soc. Am. B. 2012;**29**:335–339. DOI: 10.1364/JOSAB.29.000335

[14] Fally M, Ellaban M, Drevensek-Olenek I. Out-of-phase mixed holographic gratings: a quantitative analysis. Opt. Express. 2008;**16**:6528–6536. DOI: 10.1364/OE.16.006528

[15] Fally M, Ellaban M, Drevensek-Olenek I. Out-of-phase mixed holographic gratings: a quantitative analysis: erratum. Opt. Express. 2009;**17**:23350. DOI: 10.1364/OE.17.023350

[16] Angervaks AE, Shcheulin AS, Ryskin AI. Convertible holograms in CaF_2 crystals with color centers. Proc. SPIE. 2013;**8776**:87604. DOI: 10.1117/12.2017160

[17] Shcheulin AS, Angervaks AE, Veniaminov AV, Zakharov VV, Ryskin AI. Holograms convertible by incoherent photo-thermal treatment in CaF_2 crystals with color centers. J. Opt. Soc. Am. B. 2014;**31**:248–254. DOI: 10.1364/JOSAB.31.000248

[18] Shcheulin AS, Angervaks AE, Veniaminov AV, Fedorov PP, Kuznetsov SV, Ryskin AI. Formation of dissipative structures at hologram recording in CaF_2 crystals with color centers. Proc. SPIE. 2015;**9508**:95080D. DOI: 10.1117/12.2178477

[19] Shcheulin AS, Angervaks AE, Veniaminov AV, Zakharov VV, Fedorov PP, Ryskin AI. Self-organization of color centers in holograms recorded in CaF_2 crystals with color centers. Opt. Mater. 2015;**47**:190–195. DOI: 10.1016/j.optmat.2015.04.065

[20] Nicolis G, Prigogine I. Self-Organization in Nonequilibrium Systems. From Dissipative Structures to Order through Fluctuations. 1st ed. New York: Wiley; 1977. 512 p.

[21] Coxeter HSM. Introduction to Geometry. 2nd ed. New York: Wiley; 1989. 496 p.

[22] LeBret JB, Cramer LP, Grant Norton M, Dickinson JT. Colloid formation and laser-induced bleaching in fluorite. Appl. Phys. Lett. 2004;**85**:4382–4384. DOI: 10.1063/1.1818738

[23] Granovskii VA, Kudryavtsev MD, Ryskin AI, Shcheulin AS. Holographic prism as a new optical element: I. Principle of operation and experimental implementation. Opt. Spectrosc. 2009;**106**:774–781. DOI: 10.1134/S0030400X09050269

[24] Angervaks AE, Granovskii VA, Kudryavtsev MD, Ryskin AI, Shcheulin AS. Holographic prism as a new optical element: II. Method of measurement of reproducible angles. Opt. Spectrosc. 2010;**108**:824–830. DOI: 10.1134/S0030400X1005022X

[25] Angervaks AE, Granovskii VA, Kudryavtsev MD, Ryskin AI, Shcheulin AS. Holographic prism as a new optical element: III. Experimental implementation of a holographic prism of modification II and comparative characterization of the two holographic prism modifications from the application point of view. Opt. Spectrosc. 2012;**112**:312–317. DOI: 10.1134/S0030400X12020026

[26] Avanesov YuL, Angervaks AE, Gorokhovskii KS, Granovskii VA, Kudryavtsev MD, Kulachenkov NK, Ryskin AI, Shcheulin AS. Rotation angle measurement device: principle of operation and initial calibration results. In: Proceedings of the 11th International Multi-Conference on Systems, Signals & Devices (SSD 2014); 11–14 February 2014; Barcelona, Spain. IEEE Xplore Digital Library; 2014. 1569839857 p. DOI: 10.1109/SSD.2014.6808783

[27] Collier RJ, Burckhardt CB, Lin LH. Optical Holography. 1st ed. New York, London: Academic Press; 1971. 605 p.

IntechOpen